OPTICAL FIBER DRAWING AND DOPANT TRANSPORT

H. HUANG*, R.M. MIURA†, AND J.J. WYLIE‡

Abstract. Optical fibers are made of glass with different refractive indices in the (inner) core and the (outer) cladding regions. The difference in refractive index arises due to a rapid transition in the concentration of a dopant across the boundary between these two regions. Fibers are normally drawn from a heated glass preform, and the different dopant concentrations in the two regions will change due to dopant diffusion and convective transport induced by the flow. In this paper, we analyze a mathematical model for the dynamics of dopant concentration changes during the fiber drawing process. Using a long-wave approximation, we show that the governing equations can be reduced to a simple diffusion equation. As a result, we are able to identify key dimensionless parameters that contribute to the diffusion process. We also derive asymptotic solutions for the temperature, cross-sectional area, and effective diffusion coefficient when there are strong temperature dependencies in the viscosity and the diffusion coefficient. Our simplified model and asymptotic solutions reduce the need for extensive numerical simulations and can be used to devise control strategies to limit excess dopant diffusion.

Key words. dopant diffusion, optical fiber drawing, incompressible viscous flow, long wave approximation, asymptotic approximation.

AMS subject classifications. 76D99, 76R50, 41A60, 76D27

1. Introduction.

Optical fibers are drawn from a heated glass preform using mechanical pullers. The glass preform is fabricated so that there is a difference in the refractive index between the fiber core and the outer cladding region. This refractive index difference is achieved normally by adding a dopant to the inner core region [4]. Typically, dopant materials, such as oxides of germanium, phosphorus, and boron, are deposited in pure silica in the perform. However, during drawing, splicing, and fusion, the refractive index may change due to diffusion of the dopant in the glass [7, 11].

Compared to dopant concentration changes due to splicing and fusion of these fibers, dopant concentration changes during fiber drawing would appear to be more complicated since dopant diffusion depends not only on temperature, but on a number of other factors, including the mechanics of the drawing process. In Lyytikäinen et al. [5], numerical simulations and an experimental study of specialized fibers have been carried out. For relatively low drawing speeds, it was shown that diffusion can cause a small, but visible spreading of the dopant. It also was shown that larger drawing speeds and lower furnace temperatures both reduce the diffusion of dopant. Their simulations ignored advection of dopant by the flow and were based on a simple diffusion equation with only a radial component. Their experiments and simulations compare favorably, which indicates that the key mechanism is captured by simple radial diffusion; however, it is not clear why this is the case and whether this assumption will hold for other parameter values. On the other hand, Yan and Pitchumani [11] carried out a full numerical simulation of the drawing process, including dopant diffusion. Although the fiber surface is a free boundary, they simplified their computations by using a prescribed surface boundary based on previous numerical studies of the drawing process by Lee and Jaluria [6]. Contrary to the conclusion in Lyytikäinen [5], the numerical simulations by Yan and Pitchumani [11] show that a significant amount of diffusion occurs during the drawing process, in spite of a similar drawing environment and higher drawing speeds, which should reduce the amount of diffusion.

In this paper, we analyze a mathematical model for dopant concentration changes during optical fiber drawing. Based on an asymptotic analysis of this model, we are able to show that the diffusion of dopant is governed by a simple diffusion equation with only a radial component, as used by Lyytikäinen et al. However, the molecular diffusion coefficient used in [5] must be replaced by an effective diffusion coefficient, which includes a 'history' factor. For typical parameter values, we show that the effective diffusion coefficient is determined mainly by two dimensionless parameters, namely, the Peclet number based on the diffusion coefficient for dopant, and a parameter that quantifies the heating strength. For large changes in viscosity, we derive analytical expressions that are uniformly valid asymptotic expansions for velocity, radius, and temperature. This allows us to find simple expressions for the

*Department of Mathematics and Statistics, York University, Toronto, Ontario M3J 1P3 Canada hhuang@yorku.ca
†Department of Mathematical Sciences, New Jersey Institute of Technology, Newark, N.J. 07102 USA miura@njit.edu
‡Department of Mathematics, City University of Hong Kong, Kowloon, Hong Kong mawylie@cityu.edu.hk

effective diffusion coefficient that clearly show the way in which all of the parameters affect the diffusion process and hence reduces the need for extensive numerical simulations.

The paper is organized as follows. In Section 2, the mathematical model for glass optical fiber drawing is given and subsequently simplified. We derive explicit approximations for the temperature and cross-sectional area in Section 3. For these approximations, we considered two cases, one with cooling and one without cooling. In Section 4, we derive asymptotic approximations for the effective diffusion in the case of no cooling.

2. Problem Description. In a typical setup for glass optical fiber drawing, a cylindrical preform with radius R_0 and temperature T_0 is fed through an input nozzle into a heating and cooling device with speed u_0, see Figure 2.1. At a distance L from the input nozzle, the fiber is pulled out of the device by a roller. Between the input nozzle and a distance $L_f < L$, the fiber is inside a furnace and is subjected to heating. This heating causes the viscosity of the glass to dramatically decrease, and thus facilitates rapid stretching of the fiber with moderate forces. Between the end of the furnace and the roller, the fiber is cooled by natural and forced cooling. At the nozzle input, the dopant concentration $c = c_0(r)$ will be assumed to be a given function of the radial distance from the fiber axis, r. The aim of this study is to understand how the heating, cooling, and the stretching process, as well as the diffusion and advection of the dopant, affect the dopant concentration profile when the fiber exits the device. We note that throughout this paper, subscripts 0, f, and c refer to quantities associated with the input nozzle, furnace heating, and cooling, respectively.

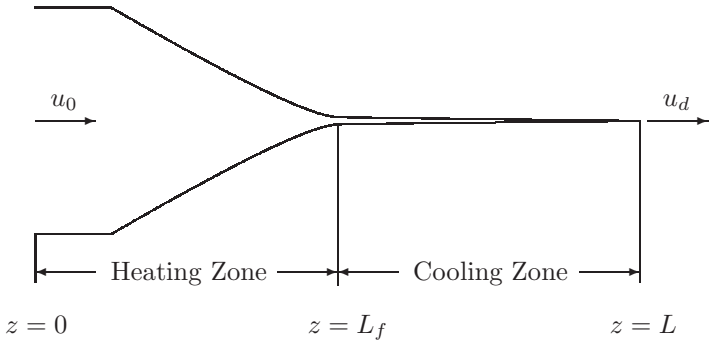

FIG. 2.1. Schematic of heating and cooling zones.

2.1. Mathematical model. We assume that the glass fiber is an incompressible fluid with temperature-dependent viscosity. Also, we assume that the dopant concentration has negligible effect on the density, viscosity, and conductivity of the glass, the fiber remains axisymmetric, and the drawing conditions are in a steady state. Under these assumptions, the governing equations for mass, momentum, energy, and dopant concentration are given by [11]

$$\frac{\partial(\rho u)}{\partial z} + \frac{1}{r}\frac{\partial(r\rho v)}{\partial r} = 0, \tag{2.1}$$

$$\frac{\partial(\rho u^2)}{\partial z} + \frac{1}{r}\frac{\partial(r\rho uv)}{\partial r} = -\frac{\partial p}{\partial z} + 2\frac{\partial}{\partial z}\left(\mu\frac{\partial u}{\partial z}\right) + \frac{1}{r}\frac{\partial}{\partial r}\left[r\mu\left(\frac{\partial u}{\partial r} + \frac{\partial v}{\partial z}\right)\right], \tag{2.2}$$

$$\frac{\partial(\rho uv)}{\partial z} + \frac{1}{r}\frac{\partial(r\rho v^2)}{\partial r} = -\frac{\partial p}{\partial r} + \frac{\partial}{\partial z}\left[\mu\left(\frac{\partial u}{\partial r} + \frac{\partial v}{\partial z}\right)\right] + \frac{2}{r}\frac{\partial}{\partial r}\left(r\mu\frac{\partial v}{\partial r}\right) - \frac{2\mu v}{r^2}, \tag{2.3}$$

$$\frac{\partial(\rho c_p uT)}{\partial z} + \frac{1}{r}\frac{\partial(r\rho c_p vT)}{\partial r} = \frac{\partial}{\partial z}\left(k\frac{\partial T}{\partial z}\right) + \frac{1}{r}\frac{\partial}{\partial r}\left(rk\frac{\partial T}{\partial r}\right), \tag{2.4}$$

$$\frac{\partial(uc)}{\partial z} + \frac{1}{r}\frac{\partial(rvc)}{\partial r} = \frac{\partial}{\partial z}\left(D\frac{\partial c}{\partial z}\right) + \frac{1}{r}\frac{\partial}{\partial r}\left(rD\frac{\partial c}{\partial r}\right), \tag{2.5}$$

where z is the distance from the input nozzle measured along the axis of the fiber, u and v are the velocity components in the axial and radial directions, respectively, p is the pressure, T is the temperature, c is

the dopant concentration, ρ is the density, μ is the viscosity, c_p is the specific heat, $k = k_T + k_R$ is the effective conductivity [11], and D is the molecular diffusivity of the dopant. We observe that the mass, momentum, and energy equations decouple from the dopant equation.

The boundary conditions at the inlet of the furnace are

$$r = R_0,\ u = u_0,\ v = 0,\ T = T_0,\ c = c_0(r) \quad \text{at} \quad z = 0. \tag{2.6}$$

At a fixed downstream location, we assume the velocity is known

$$u = u_d \quad \text{at} \quad z = L. \tag{2.7}$$

At this downstream location, boundary conditions also are needed for the radial component of the velocity v, the temperature T, and the dopant concentration c. However, we will show that in the asymptotic limit of the long wave approximation, such boundary conditions do not play a significant role outside of a thin region near this boundary. The lateral fiber surface $r = R(z)$ is a free boundary at which the following dynamic and kinematic conditions must be applied

$$\mathbf{n}^T \cdot \sigma \cdot \mathbf{n} = \Gamma\kappa,\ \mathbf{t}^T \cdot \sigma \cdot \mathbf{t} = 0,\ v = R'u \tag{2.8}$$

where the prime denotes differentiation with respect to z, σ is the stress tensor, $\mathbf{n} = [(1+R'^2)^{-1/2},\ R'(1+R'^2)^{-1/2}]^T$ is the outward normal vector to the glass surface, $\mathbf{t} = [-R'(1+R'^2)^{-1/2},\ (1+R'^2)^{-1/2}]^T$ is the corresponding vector in the tangential direction, κ is the mean curvature, and Γ is the surface tension coefficient.

The boundary condition for temperature at the fiber surface depends on whether the fiber is inside or outside of the furnace. In Lee and Jaluria [6], the heat flux q is specified when the fiber is inside the furnace. In general, q depends on many factors, such as the furnace wall temperature profile, inert gas flow, and the dimensions of the furnace, as well as the fiber temperature. We will assume that the heating/cooling follows the standard Newton's cooling law [1]

$$-k\frac{\partial T}{\partial n} = q := \begin{cases} h_f(T_f - T), & 0 \le z < L_f, \\ -h_c(T - T_c), & L_f \le z \le L, \end{cases} \tag{2.9}$$

where T_f and T_c are the furnace and background temperatures, respectively, and h_f and h_c are the heat transfer coefficients for the heating from the furnace and cooling to the background, respectively. For simplicity, we will assume that the background temperature is the same as the temperature at the nozzle input, that is $T_c = T_0$, although generalization is straightforward.

Finally, the dopant concentration satisfies the no-flux boundary condition

$$-D\frac{\partial c}{\partial n} = 0 \tag{2.10}$$

at the fiber surface $r = R(z)$ and the regularity condition

$$\frac{\partial c}{\partial r} = 0 \tag{2.11}$$

at the axis of the thread $r = 0$.

For the glass fibers used in typical optical fiber fabrication, the viscosity of the fiber varies rapidly with temperature. This rapid variation plays a fundamental role in controlling the dynamics. Empirical data for glass, [8, 3] and references therein, show that the viscosity can be well approximated by an Arrhenius formula or an exponential law. In this paper, we will use the exponential law in the form

$$\mu(T) = \mu_0 \exp\left(-G_\mu(T - T_0)\right) \tag{2.12}$$

where μ_0 is the viscosity of the thread at T_0 and G_μ is a constant. The diffusion coefficient for the dopant also is normally assumed to follow the Arrhenius formula

$$D(T) = D_\infty \exp\left(-\frac{G_D}{T}\right) \tag{2.13}$$

TABLE 2.1
List of the physical parameter values.

ρ kg/m^3	c_p J/(K kg)	k_c W/(m K)	k_r W/(m K)	Γ kg/s	h_f W/(m^2 K)	h_c W/(m^2 K)
2.23×10^3	7.538×10^2	1.130	1.2×10^1	3×10^{-1}	200	20

u_0 m/s	u_d m/s	L m	L_f m	R_0 m	T_0 K	T_f K	μ_0 kg/(m s)	G_μ K^{-1}	D_∞ m$^2/s$	G_D K
10^{-4}	1	0.5	0.1	6×10^{-3}	300	2300	10^8	2×10^{-2}	2.4×10^{-6}	3.73×10^4

where G_D is the activation energy divided by the universal gas constant and D_∞ is the diffusion coefficient at high temperatures.

2.2. Dimensional analysis. We nondimensionalize the governing equations using the following scalings

$$\hat{z} = \frac{z}{L},\ \hat{r} = \frac{r}{R_0},\ \hat{R} = \frac{R}{R_0},\ \hat{u} = \frac{u}{u_0},\ \hat{v} = \frac{Lv}{R_0 u_0},\ \hat{p} = \frac{R_0^2 p}{\mu_0 u_0 L},$$

$$\hat{\mu} = \frac{\mu}{\mu_0},\ \theta = \frac{T - T_0}{T_f - T_0},\ \hat{c_0} = \frac{c_0}{c_0(0)},\ \hat{c} = \frac{c}{c_0(0)},\ \hat{D} = \frac{D}{D_\infty}.$$

Substitution of these scalings into (2.1)–(2.4) yields the following dimensionless parameters, which we list along with their order of magnitude estimates based on the typical parameter values [5, 6, 11] that are listed in Table 2.1.

$$D_r = \frac{u_d}{u_0} \approx 10^4,\ \delta = \frac{R_0}{L} \approx 10^{-2},\ Re = \frac{\rho u_0 L}{3\mu_0} \approx 10^{-9},\ \lambda = \frac{\Gamma L}{3\mu_0 u_0 R_0} \approx 10^{-3},\ Bi = \frac{h_f R_0}{k} \approx 10^{-1},$$

$$\alpha_\mu = G_\mu(T_f - T_0) \approx 40,\ \alpha_D = \frac{G_D}{T_f - T_0} \approx 20,\ \Theta = \frac{T_0}{T_f - T_0} \approx 0.15,\ \mathcal{P} = \frac{u_0 R_0^2}{L D_\infty} \approx 3 \times 10^{-3},$$

and

$$\mathcal{H}_f = \frac{2\sqrt{\pi} h_f L}{\rho c_p u_0 R_0} \approx 350,\ \mathcal{H}_c = \frac{2\sqrt{\pi} h_c L}{\rho c_p u_0 R_0} \approx 35,\ \ell = \frac{L_f}{L} \approx 0.2.$$

Here D_r is the draw ratio, δ is the aspect ratio, Re is the Reynolds number, λ is the ratio of surface tension forces to viscous forces, and Bi is the Biot number. The parameters α_μ and α_D measure the changes in the viscosity and the diffusion coefficient as the temperature varies between its initial value and the heater temperature, respectively, Θ is the ratio of the initial temperature to the difference between the heater and initial temperatures, $\mathcal{P}$ is the Peclet number for the dopant, $\mathcal{H}_f$ and $\mathcal{H}_c$ represent the dimensionless strengths of the heating and cooling, respectively, and ℓ represents the proportion of the length of the device that is heated by the furnace. We note that the Biot number estimated here is consistent with the value cited in [6], who estimate the heat transfer based on an estimate for the heat flux.

2.2.1. Flow and temperature equations - simplifications. The mass, momentum, and temperature equations clearly decouple from the dopant equation, and we begin by simplifying these equations. Based on the parameter values given in Table 2.1, we see that δ, Re, λ, and Bi are small. Since $\delta \ll 1$, we can use the long-wave approximation. Furthermore, since $\lambda \ll 1$ and $Re \ll 1$, we can ignore

[1] Other types of heating and cooling laws, such as radiative heating and cooling can be studied using a procedure similar to that used in this paper.

the inertia and surface tension terms in the momentum equations. Finally, assuming that $Bi \ll 1$, the equations (2.1)–(2.4) become (dropping the hats)

$$\frac{\partial}{\partial z}(us) = 0, \tag{2.14}$$

$$\frac{1}{s}\frac{\partial}{\partial z}\left(\mu s \frac{\partial u}{\partial z}\right) = 0, \tag{2.15}$$

$$u\frac{\partial \theta}{\partial z} = \frac{\mathcal{H}_f(1-\theta)H(\ell - z) - \mathcal{H}_c\theta H(z-\ell)}{s^{1/2}}, \tag{2.16}$$

where H is the Heaviside step function, $s = R^2$, and

$$\mu = \exp\left(-\alpha_\mu \theta\right).$$

The derivation of these equations can be found in a number of references, cf. [1, 2, 9, 10].

The boundary conditions are given by

$$s = 1,\ u = 1,\ \theta = 0 \quad \text{at} \quad z = 0, \tag{2.17}$$

and

$$u = D_r \quad \text{at} \quad z = 1. \tag{2.18}$$

2.2.2. Dopant equation - long wave approximation. The long-wave approximation of the dopant concentration equation (2.5) is

$$\mathcal{P}\left(u\frac{\partial c}{\partial z} - \frac{r}{2}\frac{\partial u}{\partial z}\frac{\partial c}{\partial r}\right) = \frac{1}{r}\frac{\partial}{\partial r}\left(rD\frac{\partial c}{\partial r}\right) \tag{2.19}$$

where

$$D = \exp\left(-\frac{\alpha_D}{\theta + \Theta}\right). \tag{2.20}$$

The boundary conditions are

$$c = c_0(r) \quad \text{at} \quad z = 0, \tag{2.21}$$

and

$$c_r = 0 \quad \text{at} \quad r = 0 \quad \text{and} \quad r = \sqrt{s}. \tag{2.22}$$

2.2.3. Flow and temperature equations - reduced system. From (2.14), (2.15), and the boundary conditions on u and s in (2.17) and (2.18), it is easy to verify that

$$su = 1 \quad \text{and} \quad \mu s u_z = 2F \tag{2.23}$$

where

$$F = \frac{\ln D_r}{2\int_0^1 \mu^{-1} dz}$$

is the effective pulling force that will be obtained by using the boundary condition at $z = 1$. Using (2.14) and the first equation in (2.23) to eliminate u and u_z in the equation in (2.14) and the temperature equation (2.16), we obtain a system of two coupled first-order ordinary differential equations for s and θ

$$s_z = -\frac{2Fs}{\mu}, \tag{2.24}$$

$$\theta_z = s^{1/2}\left[\mathcal{H}_f(1-\theta)H(\ell - z) - \mathcal{H}_c\theta H(z-\ell)\right], \tag{2.25}$$

which must be solved subject to the following boundary conditions

$$s = 1,\ \theta = 0 \quad \text{at} \quad z = 0 \quad \text{and} \quad s = D_r^{-1} \quad \text{at} \quad z = 1. \tag{2.26}$$

2.2.4. Dopant equation - simplification. We can further simplify the equation for dopant concentration changes by defining

$$\phi(z) \equiv \int_0^z D(\theta(z')dz' \text{ and } \bar{\phi} \equiv \phi(1), \tag{2.27}$$

and using the following coordinate transformation $(z, r) \to (\tau, \xi)$ defined by

$$\xi = \frac{r}{R}, \qquad \tau = \frac{\phi(z)}{\bar{\phi}}. \tag{2.28}$$

The quantity

$$\mathcal{D} = \frac{\bar{\phi}}{\mathcal{P}} \tag{2.29}$$

will be called the effective diffusion coefficient, and we obtain

$$c_\tau = \frac{\mathcal{D}}{\xi}\frac{\partial}{\partial \xi}\left(\xi \frac{\partial c}{\partial \xi}\right) \tag{2.30}$$

subject to

$$c = c_0(\xi) \quad \text{at} \quad \tau = 0, \tag{2.31}$$

and

$$c_\xi = 0 \quad \text{at} \quad \xi = 0 \quad \text{and} \quad \xi = 1. \tag{2.32}$$

The exit of the heating and cooling device is located at $\tau = 1$.

3. Asymptotic Solution for θ and s. We consider two cases: first without cooling ($\ell = 1$) in which the furnace heats the entire thread, followed by the case with cooling ($\ell < 1$) in which the furnace heats the initial portion of the fiber whereas the remaining portion is subjected to cooling.

3.1. $\ell = 1$. Introducing the scaled effective force $\mathcal{F} = 2Fe^{\alpha_\mu}/\ln D_r$, we can rewrite the system (2.24) and (2.25) as

$$s_z = -\mathcal{F} \ln D_r s e^{-\alpha_\mu(1-\theta)}, \tag{3.1}$$

$$\theta_z = \mathcal{H}_f \sqrt{s}(1-\theta), \tag{3.2}$$

subject to boundary conditions $s(0) = 1$ and $\theta(0) = 0$. From the above two equations, we obtain

$$\frac{ds}{d\theta} = -\frac{\mathcal{F} \ln D_r}{\mathcal{H}_f} \frac{\sqrt{s} e^{-\alpha_\mu(1-\theta)}}{1-\theta}. \tag{3.3}$$

Integrating and using the boundary conditions, we obtain

$$s = \left(1 - \frac{\mathcal{F} \ln D_r}{2\mathcal{H}_f} \{E_1[\alpha_\mu(1-\theta)] - E_1[\alpha_\mu]\}\right)^2 \tag{3.4}$$

where

$$E_1[z] = \int_z^\infty \frac{e^{-x}}{x} dx$$

is the exponential integral. Note that up to this point no approximation has been made. To proceed further, we exploit the fact that viscosity varies rapidly with temperature, that is $\alpha_\mu \gg 1$. Note that the exponential integral has the following asymptotic approximations

$$E_1[z] \sim \frac{e^{-z}}{z} \text{ as } z \to \infty, \qquad E_1[z] \sim -\ln(z) - \gamma \text{ as } z \to 0$$

where $\gamma = 0.5772\ldots$ is Euler's constant.

From (3.2), we have

$$\theta_z = \mathcal{H}_f \left(1 - \frac{\mathcal{F} \ln D_r}{2\mathcal{H}_f} \left\{E_1[\alpha_\mu(1-\theta)] - E_1[\alpha_\mu]\right\}\right)(1-\theta). \tag{3.5}$$

Since $\alpha_\mu \approx 30 \gg 1$, we have $E_1[\alpha_\mu]$ is small. Also, $E_1[\alpha_\mu(1-\theta)]$ will be small if $1-\theta \ll \alpha_\mu^{-1}$. Therefore,

$$\theta_z = \mathcal{H}_f(1-\theta), \tag{3.6}$$

which can be solved to give

$$\theta = 1 - e^{-\mathcal{H}_f z}. \tag{3.7}$$

Clearly, $1-\theta \to 0$ as z increases to 1 for $\mathcal{H}_f \gg 1$. Thus, for $z \gg \mathcal{H}_f^{-1}$, we have

$$\theta_z = \mathcal{H}_f \left(1 + \frac{\mathcal{F} \ln D_r}{2\mathcal{H}_f} \left\{\ln[\alpha_\mu(1-\theta)] + \gamma\right\}\right)(1-\theta). \tag{3.8}$$

Letting

$$\alpha_\mu(1-\theta) = e^{-\frac{2\mathcal{H}_f}{\mathcal{F}\ln D_r}}\hat{\theta},$$

we have

$$\hat{\theta}_z = -\frac{\mathcal{F}\ln D_r}{2}\left(\ln\hat{\theta} + \gamma\right)\hat{\theta}, \tag{3.9}$$

which can be integrated to obtain

$$\ln\hat{\theta} = -\gamma + C_1 e^{-\frac{\mathcal{F}\ln D_r}{2}z} \tag{3.10}$$

where C_1 is an integration constant.

Next, we match the above solution with (3.6) to obtain

$$C_1 = \gamma + \ln\alpha_\mu + \frac{2\mathcal{H}_f}{\mathcal{F}\ln D_r}. \tag{3.11}$$

Thus,

$$\hat{\theta} = \exp\left[-\gamma + \left(\gamma + \ln\alpha_\mu + \frac{2\mathcal{H}_f}{\mathcal{F}\ln D_r}\right)e^{-\frac{\mathcal{F}\ln D_r}{2}z}\right], \tag{3.12}$$

or returning to the original variable,

$$\theta = 1 - \exp\left[-\left(\gamma + \ln\alpha_\mu + \frac{2\mathcal{H}_f}{\mathcal{F}\ln D_r}\right)\left(1 - e^{-\frac{\mathcal{F}\ln D_r}{2}z}\right)\right]. \tag{3.13}$$

Given θ, we can find s using (3.4).

The scaled pulling force $\mathcal{F}$ can be obtained by substituting $z=1$ into (3.13) and (3.4) and using the condition $s(1) = D_r^{-1}$. Using the fact that $\alpha_\mu \gg 1$ and the asymptotic properties of E_1, we obtain

$$\mathcal{F} = 1 + \frac{2}{\ln D_r}\ln\left[1 + \frac{\mathcal{F}(\ln\alpha_\mu + \gamma)\ln D_r}{2\mathcal{H}_f}\right]. \tag{3.14}$$

In general, to obtain $\mathcal{F}$, this equation must be solved numerically. But for typical parameter values, we have

$$\frac{(\ln\alpha_\mu + \gamma)\ln D_r}{2\mathcal{H}_f} \sim 10^{-1} \ll 1, \tag{3.15}$$

and so we can obtain an asymptotic estimate for $\mathcal{F}$ in closed form

$$\mathcal{F} = 1 + \frac{\ln\alpha_\mu + \gamma}{\mathcal{H}_f}. \tag{3.16}$$

In Figure 3.1, we plot the asymptotic and numerical solutions, and it can be seen that the agreement between the two solutions is excellent.

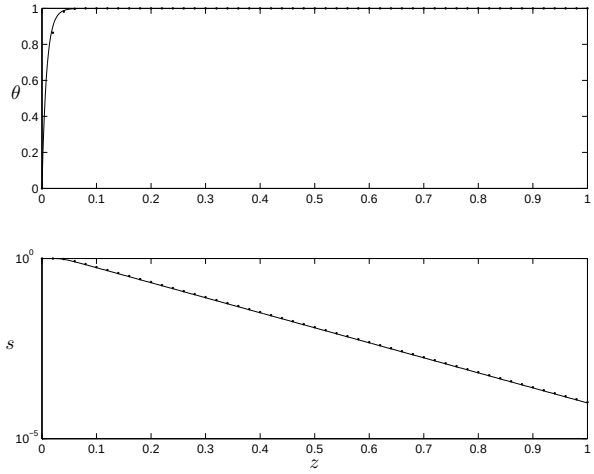

FIG. 3.1. Numerical (dots) vs asymptotic (lines) solutions. The parameter values are: $\mathcal{H}_f = 100$, $\alpha_\mu = 30$, and $D_r = 10^4$.

3.2. $\ell < 1$**.** When there is cooling, the previous solution is valid up to the location $z = \ell$, but for $z > \ell$, the area and temperature are determined from (2.24) and (2.25)

$$s_z = -\mathcal{F}\ln(D_r)e^{\alpha_\mu(\theta-1)}s, \tag{3.17}$$

$$\theta_z = -\mathcal{H}_c\sqrt{s}\theta \tag{3.18}$$

subject to the boundary conditions $s(\ell) = s_\ell$ and $\theta(\ell) = \theta_\ell$.

We rescale the variables using

$$\vartheta = \alpha_\mu(\theta_\ell - \theta), \quad \mathfrak{s} = \sqrt{\frac{s}{s_\ell}}, \quad y = \frac{\mathcal{F}\ln(D_r)e^{\alpha_\mu(\theta_\ell-1)}}{2}(z-\ell),$$

and equations (3.17) and (3.18) become

$$\mathfrak{s}_y = -\mathfrak{s}e^{-\vartheta}, \tag{3.19}$$

$$\vartheta_y = \mathcal{A}\mathfrak{s}(1-\epsilon\vartheta) \tag{3.20}$$

where

$$\mathcal{A} = \frac{2\sqrt{s_\ell}\mathcal{H}_c\alpha_\mu\theta_\ell e^{\alpha_\mu(1-\theta_\ell)}}{\mathcal{F}\ln(D_r)}, \quad \epsilon = \frac{1}{\alpha_\mu\theta_\ell} \ll 1,$$

and subject to $\vartheta(0) = 0$ and $\mathfrak{s}(0) = 1$.

From (3.19) and (3.20), we can obtain

$$\frac{d\vartheta}{d\mathfrak{s}} = -\mathcal{A}(1-\epsilon\vartheta)e^{\vartheta}. \tag{3.21}$$

Using $\vartheta(0) = 0$, $\mathfrak{s}(0) = 1$, and integration by parts, we obtain

$$\mathfrak{s} = 1 - \frac{1}{\mathcal{A}}\int_0^\vartheta \frac{e^{-w}}{1-\epsilon w}dw = 1 + \frac{1}{\mathcal{A}}\left(\frac{e^{-\vartheta}}{1-\epsilon\vartheta} - 1\right) - \frac{\epsilon}{\mathcal{A}}\int_0^\vartheta \frac{e^{-w}}{(1-\epsilon w)^2}dw. \tag{3.22}$$

Given typical parameter values, one can readily see that the scaled temperature ϑ at the exit is much greater than ϵ^{-1}. Therefore, $\epsilon/(1-\epsilon\vartheta) \ll 1$, and equation (3.22) can be approximated as

$$\mathfrak{s} = 1 + \frac{1}{\mathcal{A}}\left(\frac{e^{-\vartheta}}{1-\epsilon\vartheta} - 1\right). \tag{3.23}$$

We now proceed with three different cases: $\mathcal{A} = 1$, $\mathcal{A} < 1$, and $\mathcal{A} > 1$.

Case 1. $\mathcal{A} = 1$**.** In this case, we have

$$\mathfrak{s} = e^{-\vartheta} \tag{3.24}$$

and the equation for ϑ becomes

$$\vartheta_y = e^{-\vartheta}, \tag{3.25}$$

which can be solved as

$$\vartheta = \ln(y+1) \tag{3.26}$$

using the boundary condition $\vartheta(0) = 0$. Thus, the leading-order solution for $\mathfrak{s}$ is

$$\mathfrak{s} = \frac{1}{(y+1)}. \tag{3.27}$$

Case 2. $\mathcal{A} < 1$**.** Note that $\mathcal{A}$ is the scaled cooling strength, and when $\mathcal{A} < 1$, we expect that the temperature is bounded below by $\mathcal{A} = 1$. Using the solution in **Case 1**, we note that ϑ is a monotonically increasing function with a maximum value

$$\vartheta_{max} = \ln\left(\frac{\mathcal{F}\ln(D_r)e^{\alpha_\mu(\theta_\ell - 1)}}{2}(1-\ell) + 1\right). \tag{3.28}$$

The quantity ϑ_{max} is an order one quantity as long as $\ln(\ln(D_r)) \ll \epsilon^{-1}$, so we conclude that ϑ also will be an order one quantity.

Having established that ϑ =O(1), we can approximate (3.23) by

$$\mathfrak{s} = 1 + \frac{1}{\mathcal{A}}\left(e^{-\vartheta} - 1\right). \tag{3.29}$$

From (3.20), we obtain

$$\vartheta_y = \mathcal{A}\mathfrak{s} = e^{-\vartheta} + \mathcal{A} - 1, \tag{3.30}$$

which can be integrated to give

$$\vartheta = \ln\frac{\mathcal{A}e^{(\mathcal{A}-1)y} - 1}{\mathcal{A} - 1} \tag{3.31}$$

after applying the condition $\vartheta(0) = 0$. Note that this solution also applies to the case of $\mathcal{A} = 1$ by taking the limit $\mathcal{A} \to 1$, which yields (3.26). The solution for $\mathfrak{s}$ can be obtained as

$$\mathfrak{s} = \frac{\mathcal{A} - 1}{\mathcal{A} - e^{-(\mathcal{A}-1)y}}. \tag{3.32}$$

Case 3. $\mathcal{A} > 1$**.** In this case, we need to consider two scenarios: when ϑ =O(1) and when ϑ is large.

(i). $\vartheta = O(1)$. When $\vartheta = O(1)$, the analysis is identical to the case for $A < 1$, yielding the same formulas (3.31) and (3.32).

(ii). *Large* ϑ. When $1 \ll \vartheta \ll \epsilon^{-1}$ and $\mathcal{A} > 1$, the approximation of (3.23), neglecting exponentially small terms, is given by

$$\mathfrak{s} = 1 - \frac{1}{\mathcal{A}}, \tag{3.33}$$

which can be combined with (3.20) to yield

$$\vartheta_y = (\mathcal{A} - 1)(1 - \epsilon\vartheta). \tag{3.34}$$

This equation can be solved as

$$\vartheta = \frac{1 - C_2 e^{-\epsilon(\mathcal{A}-1)y}}{\epsilon} \tag{3.35}$$

where C_2 is an integration constant. Since we obtained the solution based on the assumption that ϑ is not small, we cannot use the boundary condition $\vartheta(0) = 0$. To determine C_2, we need to match the small ϑ solution given by (3.31) with that for large ϑ given by (3.35). Taking the limit of $\vartheta \to 0$ from (3.35), we obtain

$$\vartheta \sim \frac{1 - C_2(1 - \epsilon(\mathcal{A}-1)y)}{\epsilon}.$$

For large ϑ, i.e., $y \to 0$, (3.31) gives

$$\vartheta \sim (\mathcal{A}-1)y + \ln\frac{\mathcal{A}}{\mathcal{A}-1}.$$

Comparing the two expressions, the only choice we have is

$$C_2 = 1 - \epsilon \ln\frac{\mathcal{A}}{\mathcal{A}-1},$$

and the solution becomes

$$\vartheta = \frac{1 - e^{-\epsilon(\mathcal{A}-1)y}}{\epsilon} + \left(\ln\frac{\mathcal{A}}{\mathcal{A}-1}\right) e^{-\epsilon(\mathcal{A}-1)y}. \tag{3.36}$$

Note that when $\mathcal{A} \gg 1$, $C_2 \sim 1$ and ϑ can be approximated by

$$\vartheta = \frac{1 - e^{-\epsilon(\mathcal{A}-1)y}}{\epsilon}. \tag{3.37}$$

(iii). *Uniformly valid solution.* The uniformly valid solution for ϑ obtained by combining the solutions for small and large values of ϑ is given by

$$\begin{aligned}\vartheta = \ln\frac{\mathcal{A}e^{(\mathcal{A}-1)y} - 1}{\mathcal{A}-1} + \frac{1 - e^{-\epsilon(\mathcal{A}-1)y}}{\epsilon} + \ln\frac{\mathcal{A}}{\mathcal{A}-1} e^{-\epsilon(\mathcal{A}-1)y} \\ -(\mathcal{A}-1)y - \ln\frac{\mathcal{A}}{\mathcal{A}-1}.\end{aligned} \tag{3.38}$$

The solution for $\mathfrak{s}$ can be obtained using (3.23).

Solutions in original variables. Using the original variables and $\theta = \theta_\ell - \alpha_\mu^{-1}\vartheta$, the temperature solution is given by

$$\theta = \theta_\ell - \frac{1}{\alpha_\mu}\ln\frac{\mathcal{A}\exp\left[(\mathcal{A}-1)\mathcal{B}(z-\ell)\right] - 1}{\mathcal{A}-1} \tag{3.39}$$

for $\mathcal{A} \le 1$ and

$$\begin{aligned}\theta = \theta_\ell - \frac{1}{\alpha_\mu}\ln\frac{\mathcal{A}\exp\left[(\mathcal{A}-1)\mathcal{B}(z-\ell)\right] - 1}{\mathcal{A}-1} \\ - \left(\theta_\ell - \frac{1}{\alpha_\mu}\ln\frac{\mathcal{A}}{\mathcal{A}-1}\right)\left(1 - \exp\left[-\frac{(\mathcal{A}-1)\mathcal{B}}{\alpha_\mu\theta_\ell}(z-\ell)\right]\right) + \frac{1}{\alpha_\mu}(\mathcal{A}-1)\mathcal{B}(z-\ell)\end{aligned} \tag{3.40}$$

for $\mathcal{A} > 1$. Here $\mathcal{B} = \mathcal{F}\ln(D_r)e^{\alpha_\mu(\theta_\ell - 1)}/2$.

In both cases, the solution for the cross-sectional area in the original variables is obtained using (3.23)

$$s = s_\ell\left(1 - \frac{1}{\mathcal{A}} + \frac{\theta_\ell \exp[\alpha_\mu(\theta - \theta_\ell)]}{\mathcal{A}\theta}\right)^2. \tag{3.41}$$

Using $s(1) = D_r^{-1}$, we can obtain $\mathcal{F}$ (and F) by solving the following equation numerically

$$D_r^{-1} = s_\ell \left(1 - \frac{1}{\mathcal{A}} + \frac{\theta_\ell \exp[\alpha_\mu(\theta(1) - \theta_\ell)]}{\mathcal{A}\theta(1)}\right)^2 \tag{3.42}$$

where $\theta(1)$ is evaluated at $z = 1$ using (3.39) or (3.40), depending on the value of $\mathcal{A}$.

In Figures 3.2 and 3.3, we have plotted both the numerical and the asymptotic solutions for various values of the draw ratio D_r and for two different values of the cooling parameter $\mathcal{H}_c$, respectively. It can be seen that the solutions agree very well with each other.

4. Dopant Diffusion. Since dopant transport follows a standard diffusion equation, the solution is completely determined by the effective diffusion coefficient. When the diffusion coefficient is small (as in the case of dopant diffusion), the effect of the boundary on the dopant distribution is also small. Therefore, we can ignore the boundary and solve equation (2.30) on an infinite domain as an approximation[2]. In this case, the solution for the dopant concentration can be written as

$$c(\tau, \xi) = 2\pi \int_0^1 G(\tau, \xi; \eta) c_0(\eta) \eta d\eta. \tag{4.1}$$

If we know the value of $\mathcal{D}$, then the Green's function is given by

$$G(\tau, \xi; \eta) = \frac{1}{4\pi\mathcal{D}\tau} \exp\left(-\frac{\xi^2 + \eta^2}{4\mathcal{D}\tau}\right) I_0\left(\frac{\xi\eta}{2\mathcal{D}\tau}\right) \tag{4.2}$$

where I_0 is the modified Bessel function of the first kind.

In order to illustrate how the effective diffusion coefficient $\mathcal{D}$ is affected by various parameter values, we obtain an asymptotic approximation for the case with no cooling ($\ell = 1$). Recall that in this case, the temperature is given by (3.13)

$$\theta = 1 - \exp\left[-C_1\left(1 - e^{-\frac{\mathcal{F}\ln D_r}{2} z}\right)\right],$$

with C_1 given by (3.11) and the effective diffusion coefficient is given by $\mathcal{D} = \bar{\phi}/\mathcal{P}$ where $\bar{\phi}$ is given by (2.27) with D given by (2.20).

Introducing new variables $\zeta = 1 - \exp\left(-\frac{\mathcal{F}\ln D_r}{2} z\right)$ and $\varphi(\zeta) \equiv \phi(z)$, we have

$$d\zeta = \frac{\mathcal{F}\ln D_r}{2}(1 - \zeta) dz$$

and

$$\varphi_\zeta = \frac{2}{\mathcal{F}\ln D_r} \frac{\exp\left(-\frac{\alpha_D}{\Theta + 1 - \exp(-C_1\zeta)}\right)}{1 - \zeta}, \quad \varphi(0) = 0. \tag{4.3}$$

Since $C_1 \gg 1$, the solution can be found for two cases: when $\zeta \sim C_1^{-1}$ and when $\zeta \sim 1$.

Case I. $\zeta \sim C_1^{-1} \ll 1$**.** In this case, we use a new variable $\hat{\zeta} = C_1\zeta$ and denote the solution by $\varphi^{(i)}$ (inner solution) which satisfies

$$\varphi^{(i)}_{\hat{\zeta}} = \frac{2\exp\left(-\frac{\alpha_D}{\Theta + 1 - \exp(-\hat{\zeta})}\right)}{C_1\mathcal{F}\ln D_r}, \quad \varphi^{(i)}(0) = 0. \tag{4.4}$$

[2]If we consider the boundary effect, we can use the series solution given by

$$c(\tau, \xi) = 2\left[1 + \frac{r_*}{R}\sum_{m=1}^{\infty} e^{-\lambda_m^2 \mathcal{D}\tau} \frac{J_0(\lambda_m \xi) J_1(\lambda_m r_* R^{-1})}{\lambda_m J_0(\lambda_m)^2}\right]$$

where λ_m are the zeros of $J_1(\lambda)$. As long as the diffusion is not too small, only a small number of terms are needed. For small diffusion coefficient values, convergence becomes slow, and we can switch to the solution based on the infinite domain Green's function.

The inner solution can be obtained as

$$\varphi^{(i)}(\hat{\zeta}) = -\frac{2}{C_1\mathcal{F}\ln D_r}\left[E_1(x) - \exp\left(-\frac{\alpha_D}{\Theta+1}\right)E_1\left(x-\frac{\alpha_D}{\Theta+1}\right)\right]_{x=\alpha_D/\Theta}^{x=\alpha_D/(\Theta+1-\exp(-\hat{\zeta}))}. \tag{4.5}$$

Case II. $\zeta \sim 1$**.** In this case, we denote the solution by $\varphi^{(o)}$ (outer solution) which satisfies

$$\varphi_\zeta^{(o)} = \frac{2}{\mathcal{F}\ln D_r}\frac{\exp(-\frac{\alpha_D}{\Theta+1})}{1-\zeta}. \tag{4.6}$$

The solution can be obtained as

$$\varphi^{(o)}(\zeta) = -\frac{2\exp(-\frac{\alpha_D}{\Theta+1})}{\mathcal{F}\ln D_r}\ln(1-\zeta) + C_3 \tag{4.7}$$

where C_3 is an integration constant.

Matching. To determine the integration constant C_3 and the outer solution, $\varphi^{(o)}$, we need to match the two solutions as follows

$$\lim_{\hat{\zeta}\to\infty}\varphi^{(i)}(\hat{\zeta}) = \lim_{\zeta\to 0}\varphi^{(o)}(\zeta).$$

Since

$$\varphi^{(o)}(\zeta) \sim C_3 + \frac{2\exp(-\frac{\alpha_D}{\Theta+1})}{\mathcal{F}\ln D_r}\zeta \quad \text{as} \quad \zeta\to 0 \tag{4.8}$$

and $E_1[z] \sim -\gamma - \ln(z)$ for small z, we have

$$\begin{aligned}
\varphi^{(i)}(\hat{\zeta}) \sim & -\frac{2}{C_1\mathcal{F}\ln D_r}\left\{E_1\left(\frac{\alpha_D}{\Theta+1}\right) - E_1\left(\frac{\alpha_D}{\Theta}\right) - \exp\left(-\frac{\alpha_D}{\Theta+1}\right)\left[-\gamma - \ln\left(\frac{\alpha_D}{\Theta+1-\exp\left(-\hat{\zeta}\right)}\right.\right.\right. \\
& \left.\left.\left. -\frac{\alpha_D}{\Theta+1}\right)\right] + \exp\left(-\frac{\alpha_D}{\Theta+1}\right)E_1\left(\frac{\alpha_D}{\Theta}-\frac{\alpha_D}{\Theta+1}\right)\right\} \\
\approx & -\frac{2}{C_1\mathcal{F}\ln D_r}\left\{E_1\left(\frac{\alpha_D}{\Theta+1}\right) - E_1\left(\frac{\alpha_D}{\Theta}\right) - \exp\left(-\frac{\alpha_D}{\Theta+1}\right)\left[-\gamma - \ln\alpha_D + \hat{\zeta} + 2\ln(\Theta+1)\right]\right. \\
& \left. + \exp\left(-\frac{\alpha_D}{\Theta+1}\right)E_1\left(\frac{\alpha_D}{\Theta(\Theta+1)}\right)\right\} \\
\approx & -\frac{2}{C_1\mathcal{F}\ln D_r}\left\{E_1\left(\frac{\alpha_D}{\Theta+1}\right) - E_1\left(\frac{\alpha_D}{\Theta}\right) - \exp\left(-\frac{\alpha_D}{\Theta+1}\right)[-\gamma - \ln\alpha_D + 2\ln(\Theta+1)]\right. \\
& \left. + \exp\left(-\frac{\alpha_D}{\Theta+1}\right)E_1\left(\frac{\alpha_D}{\Theta(\Theta+1)}\right)\right\} + \frac{2\exp\left(-\frac{\alpha_D}{\Theta+1}\right)}{\mathcal{F}\ln D_r}\frac{\hat{\zeta}}{C_1} \quad \text{as} \quad \hat{\zeta}\to\infty.
\end{aligned} \tag{4.9}$$

We obtain

$$\begin{aligned}
C_3 = & -\frac{2}{C_1\mathcal{F}\ln D_r}\left\{E_1\left(\frac{\alpha_D}{\Theta+1}\right) - E_1\left(\frac{\alpha_D}{\Theta}\right) - \exp\left(-\frac{\alpha_D}{\Theta+1}\right)[-\gamma - \ln\alpha_D + 2\ln(\Theta+1)]\right. \\
& \left. + \exp\left(-\frac{\alpha_D}{\Theta+1}\right)E_1\left(\frac{\alpha_D}{\Theta(\Theta+1)}\right)\right\}.
\end{aligned} \tag{4.10}$$

Using the original variable, we have

$$\phi^{(o)}(z) = \exp\left(-\frac{\alpha_D}{\Theta+1}\right)z + C_3, \tag{4.11}$$

from which we obtain the effective diffusion coefficient as

$$\mathcal{D} = \frac{\exp\left(-\frac{\alpha_D}{\Theta+1}\right) + C_3}{\mathcal{P}}. \tag{4.12}$$

First, we observe that the leading order part of $\mathcal{D}$ is given by $\mathcal{P}^{-1}\exp\left(-\frac{\alpha_D}{\Theta+1}\right)$, which is the value of the effective diffusion coefficient when $\theta = \Theta$ for all z. The correction term C_3 is inversely proportional to

$$2\mathcal{H}_f + (\ln\alpha_\mu + \gamma)\left(1 + \frac{\ln\alpha_\mu + \gamma}{\mathcal{H}_f}\right)\ln D_r$$

which is only weakly dependent on the draw ratio D_r since $\mathcal{H}_f$ is typically much larger than the other parameters.

On the other hand, $\mathcal{D}$ is strongly affected by the Peclet number $\mathcal{P}$. Therefore, the most effective way to control excessive diffusion is to increase $\mathcal{P}$, which can be achieved by using relatively large feeding speed. We note that the diffusion coefficient given here is for the scaled fiber radius. Thus, the absolute length of diffusion is proportional to the fiber radius.

Finally, to find $\mathcal{D}$ for the case with cooling, we could solve for the temperature from (2.24)-(2.25) with boundary condition (2.26). The effective diffusion coefficient could be computed using the integral $\int_0^1 D(\theta)dz$. In general, we can apply numerical methods, e.g., finite difference to solve the flow and temperature equations (2.24) and (2.25) and numerical quadrature to the integral to find an approximation of $\mathcal{D}$. However, since we already obtained an asymptotic solution for the temperature, $\mathcal{D}$ can be computed easily by evaluating the integral using numerical quadrature.

5. Conclusion. In this paper, we have shown that the long-wave approximation can be used to dramatically simplify the governing equations for dopant transport in optical fiber drawing. The viscosity and diffusion coefficient vary rapidly with temperature, which makes direct numerical simulations difficult. However, we take advantage of these rapid changes to derive asymptotic approximations of the solution. We show that the transport of dopant satisfies a simple diffusion equation with an effective diffusion coefficient that can be computed easily using our asymptotic solution. Our solution shows that the feeding speed is the most effective way to control dopant diffusion from the core into the cladding region. Using our asymptotic solution, other control strategies can also be developed.

REFERENCES

[1] A.D. Fitt, K. Furusawa, T.M. Monro, and C.P. Please, *Modeling the fabrication of hollow fibers: Capillary drawing.* J. Lightwave Technologies, **19** (2001), pp. 1924-1931.

[2] G. Gupta and W.W. Schultz, *Non-isothermal flows of Newtonian slender glass fibers.* Int. J. Nonlinear Mech. **33** (1998), pp. 151–163.

[3] H. Huang, R.M. Miura, W.P. Ireland, and E. Puil, Heat-induced stretching of a glass tube under tension. SIAM J. Appl. Math., **63** (2003), pp. 1499-1519.

[4] T. Izawa, *Early days of VAD process.* IEEE J. Selected Topics Quantum Electronics, **6** (2000), pp. 1220-1227.

[5] K. Lyytikäinen, S.T. Huntington, A.L.G. Carter, P. McNamara, S. Fleming, J. Abramczyk, I. Kaplin, G. Schötz, *Dopant diffusion during optical fibre drawing.* Optical Express, **12** (2004), pp. 972-977.

[6] S.H.-K. Lee and Y. Jaluria, *Effects of variable properties and viscosity dissipation during optical fiber drawing.* Trans. ASME, **118** (1996), pp. 350-358.

[7] E. Pone, X. Daxhelet, and S. Lacroix, *Refractive index profile of fused-fiber couplers cross-section.* Optical Express, **12** (2004), pp. 1036-1044.

[8] H. Scholze, *Glass, Nature, Structure, and Properties*, translated by M.J. Lakin, Springer-Verlag, New York, 1990, pp. 255-272.

[9] J. Wylie and H. Huang, *Extensional flows with viscous heating.* J. Fluid Mech., **570** (2007), pp. 359-370.

[10] J. Wylie, H. Huang, and R.M. Miura, *Thermal instability in drawing viscous threads.* J. Fluid Mech., **570** (2007), pp. 1-13.

[11] Y. Yan and R. Pitchumani, *Numerical study on the dopant concentration and refractive index profile evolution in an optical fiber manufacturing process.* Int. J. Heat Mass Transfer, **49** (2006), pp. 2097-2112.

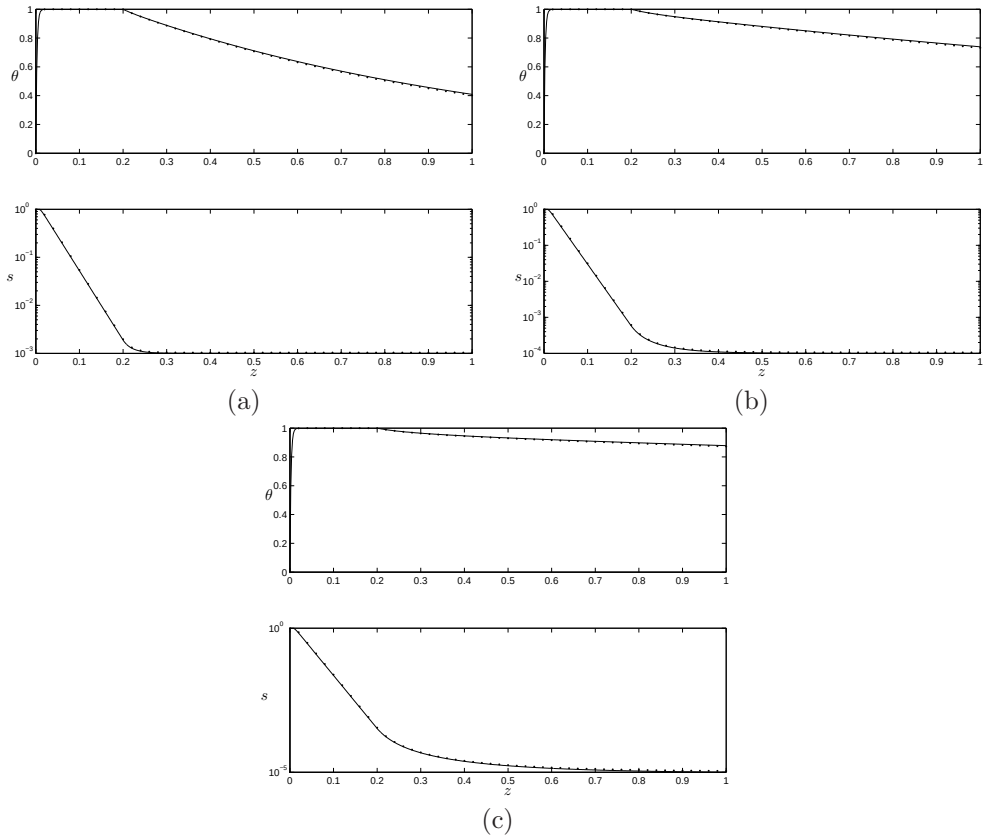

FIG. 3.2. Numerical (dots) vs asymptotic solutions (solid line) given by (3.40) and (3.41): (a) $D_r = 10^3$ ($\mathcal{A} = 3.67$); (b) $D_r = 10^4$ ($\mathcal{A} = 1.71$); and (c) $D_r = 10^5$ ($\mathcal{A} = 1.20$). Values of other parameters are: $\mathcal{H} = 350$, $\mathcal{H}_c = 35$, $\alpha_\mu = 40$, $\ell = 0.2$.

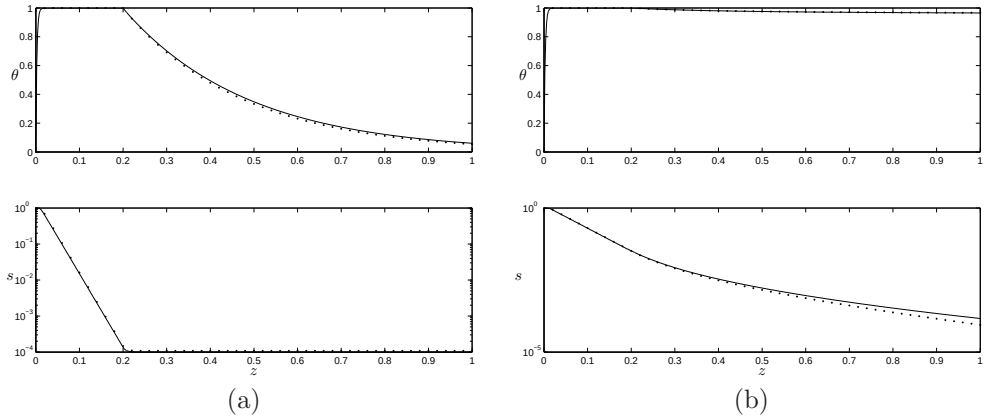

FIG. 3.3. Numerical (dots) vs asymptotic solutions (solid line) given by (3.39), (3.40), and (3.41): (a) $\mathcal{H}_c = 350$ ($\mathcal{A} = 6.96$); and (b) $\mathcal{H}_c = 1$ ($\mathcal{A} = 0.78$). Values of other parameters are: $\mathcal{H} = 350$, $D_r = 10^4$, $\alpha_\mu = 40$, $\ell = 0.2$.